Carbon 145 (2019) 549–555

Contents lists available at ScienceDirect

Carbon

journal homepage: www.elsevier.com/locate/carbon

Differences in self-assembly of spherical C_{60} and planar PTCDA on rippled graphene surfaces

Yanlong Li [a, 1], Xiaoyang Liu [b, 1], Chuanhui Chen [a, c], James Duchamp [b], Rong Huang [b], Ting-Fung Chung [d], Maxwell Young [a], Tarek Chalal [a], Yong P. Chen [d, e, f], James R. Heflin [a], Harry C. Dorn [b, *], Chenggang Tao [a, c, **]

[a] Department of Physics, Virginia Tech, Blacksburg, VA, 24061, United States
[b] Department of Chemistry, Virginia Tech, Blacksburg, VA, 24061, United States
[c] Center for Soft Matter and Biological Physics, Virginia Tech, Blacksburg, VA, 24061, United States
[d] Department of Physics and Astronomy, Purdue University, West Lafayette, IN, 47907, United States
[e] School of Electrical and Computer Engineering and Purdue Quantum Center, Purdue University, West Lafayette, IN, 47907, United States
[f] WPI-AIMR International Research Center on Materials Science, Tohoku University, Sendai, 980-8577, Japan

ARTICLE INFO

Article history:
Received 23 October 2018
Received in revised form
31 December 2018
Accepted 17 January 2019
Available online 22 January 2019

ABSTRACT

It was recently recognized that two-dimensional (2D) graphene exhibits nonplanar aberrations such as a rippled surface. Understanding the self-assembly of organic semiconductor molecules on monolayer 2D curved graphene surfaces is a paramount issue for ultimate application in semiconductor and opto-electronic devices. Herein, we report on the preparation of fullerene, C_{60} and perylenetetracarboxylic dianhydride (PTCDA) molecules adsorbed on a rippled graphene surface. We find that the spherical C_{60} molecules form a quasi-hexagonal close packed (hcp) structure, while the planar PTCDA molecules form a disordered herringbone structure. These 2D layer systems have been characterized by experimental scanning tunneling microscope (STM) imaging and computational density functional theory (DFT) approaches. The DFT computational results exhibit interaction energies for adsorbed molecule/rippled graphene complexes located in the 2D graphene valley sites that are significantly larger in comparison with adsorbed idealized planar/molecule graphene 2D complexes. In addition, we report that the adsorbed PTCDA molecules prefer different orientations when the rippled graphene peak regions are compared to the valley regions. This difference in orientations causes the PTCDA molecules to form a disordered herringbone structure on the rippled graphene surface. The results of this study clearly illustrate significant differences in C_{60} and PTCDA molecular packing on rippled graphene surfaces.

1. Introduction

Graphene is a unique two-dimensional (2D) material that exhibits fascinating physical and chemical properties and has a wide range of applications [1–3]. For instance, thanks to its single-atom thickness and flexibility, graphene is an excellent candidate for flexible electronics, textures and gas sensors [4–9]. To optimize the applications of graphene and other 2D materials, it is essential to investigate how curvature affects and tunes their properties. It has been reported that graphene on rough substrates (e.g. SiO_2) or suspended exhibits nonplanar aberrations [10,11]. Furthermore, rippling the graphene to induce a curved surface would introduce variability into the properties of graphene and changes interactions with adsorbed molecules, which has not been experimentally examined.

Significant research efforts have recently been devoted to investigate the adsorption and desorption of various molecules on planar graphene and other 2D materials, such as fabricating and tuning molecule/graphene hybrid structures [12–16]. Among the organic species, C_{60} and perylenetetracarboxylic dianhydride (PTCDA) have attracted a huge amount of research interest partially because they are key components, as effective acceptors, in photovoltaic cells [12,16–24]. In the past two decades the power conversion efficiency of organic solar cells has rapidly increased,

* Corresponding author.
** Corresponding author. Department of Physics, Virginia Tech, Blacksburg, VA, 24061, United States.
E-mail addresses: hdorn@vt.edu (H.C. Dorn), cgtao@vt.edu (C. Tao).
[1] These authors contributed equally to this work.

https://doi.org/10.1016/j.carbon.2019.01.070
0008-6223/

currently beyond 17% [25]. To further improve the efficiency of organic cells, it is necessary to understand the interactions between the organic species and other building blocks like graphene, which is an excellent material for transparent electrodes in solar cells [26,27]. Development and study of hybrid nanostructures based on rippled graphene, C_{60}/rippled graphene, and PTCDA/rippled graphene could provide significant insights for improving the efficiency of organic solar cells.

Previous experimental and computational studies have found that C_{60} and PTCDA on a planar graphene surface form a hexagonal close packed (hcp) structure and a herringbone structure, respectively [12,13,16–19,28,29]. The major interaction present in the C_{60}/planar graphene system is a π-π stacking interaction [30]. The π-π stacking interactions are common in parallel aromatic systems, have distances ranging from 3.0 to 4.0 Å and are mainly based on van der Waals forces [31,32]. The PTCDA/graphene system also contains π-π stacking interactions, but the dominant interaction that leads to a herringbone pattern is intermolecular hydrogen bonding [17]. We now report significant experimental and computational differences of spherical C_{60} and planar PTCDA self-assembled structures on rippled graphene surfaces. The inherent ability to tune the interactions between rippled graphene and structurally different molecules will undoubtedly open the door to interesting properties and potential applications of curved 2D materials, such as flexible sensors [33–36].

2. Experimental and computational methods

Experimental: All STM measurements were carried out in an ultra-high vacuum (UHV) scanning tunneling microscope system (Omicron RT-STM). Before C_{60} deposition, the graphene was grown using chemical vapor deposition (CVD) onto Cu foil [37] and annealed for 12 h at 673 K in a preparation chamber with a base pressure of 1×10^{-10} torr. PTCDA powder (TCI AMERICA, 99.0% purity) was loaded into the homemade Knudsen cell and mounted in the load lock side A of the STM system. C_{60} powder (MER Corporation, 99.5% purity) was loaded into the homemade Knudsen cell and mounted in the load lock side B of the STM system. The C_{60} and PTCDA sources were degassed to 1×10^{-6} torr prior to deposition. C_{60} and PTCDA molecules were then simultaneously deposited onto graphene at a deposition rate of ~0.5 monolayer/min with the background pressure below 1.8×10^{-8} torr. During the deposition process, the substrate was kept at 413 K. The sample was subsequently annealed at 423 K for 1 h in the preparation chamber of the STM system with a base pressure of 1.0×10^{-10} torr. All of the STM measurements were performed at room temperature with a base pressure of 1.9×10^{-10} torr. The STM used a chemically etched tungsten tip.

Computational: Density functional theory (DFT) based calculations are used to obtain further understanding of the self-assembled systems. A model containing an adsorbed molecule and a curved graphene surface is used to simulate the attachment of C_{60} and PTCDA on the rippled graphene surface. The structures of C_{60} and PTCDA are fully optimized at B3LYP level with def2-SVP basis set as provided in ORCA 3.0.3. The curved graphene is constructed based on experiment observation and then is optimized with constraints to maintain the bending angles and size. The energies of combined system are estimated based on single point calculations [38–40]. DFT based approaches with D3-correction are used to address the intermolecular interactions between the C_{60} and PTCDA molecules and the graphene [41,42]. The distance between C_{60} and the curved graphene surface are changed consistently and system energy for each distance is calculated. The energy of C_{60}/curved graphene complex is sensitive to the orientation of the C_{60} molecules on graphene. To solve the orientation-related challenge, we employed a detailed minimum potential search on representative orientations [43,44]. Comparative calculations with molecules adsorbed on planar graphene are also reported. Additional computational details are presented in the Supporting Information.

3. Results and discussion

The self-assembled structure of molecules adsorbed on graphene relates to the geometry of graphene underneath. We identified three different patterns of graphene: planar graphene labeled as I (Fig. 1h and i)), one-dimensional (1D)-rippled graphene labeled as II (Fig. 1a–d), 2D-rippled graphene labeled as III (Fig. 1e and f). Planar graphene usually forms a moiré pattern on Cu substrate. Fig. 1i shows a moiré pattern with a hexagonal moiré super lattice with periodicity of 2.0 nm. Besides the planar graphene areas, we also observed 1D-rippled graphene (Fig. 1a–c). Fig. 1a shows the coexistence of planar graphene (I) and 1D-rippled graphene (II). Fig. 1d, a line profile of blue line in Fig. 1b, shows a periodicity of ~5 nm with amplitude of 0.23 nm. Typically, the peaks of the rippled graphene have heights that range from 0.2 nm to 0.4 nm and periodicities that range from 3 nm to 10 nm. High resolution STM images (Fig. 1c and Supporting Information Figs. S1d and S1e) reveal a honeycomb lattice of graphene on the top of each ripple. For 2D-rippled graphene (Fig. 1e and f), the ripples are along two perpendicular directions with the peak height and periodicity similar to 1D-rippled graphene. Considering the heights of the ripples are much higher than the surface smoothness of the underneath Cu(111), Cu(100) or Cu(110) that is in the range of less than 0.1 nm [34,45], the line profiles of the ripples (Supporting Information Fig. S1 b, c) indicate that the graphene in these areas is quasi-suspended over the Cu substrate.

The formation of rippled graphene is mainly due to the negative thermal expansion coefficient of graphene [34,35,45]. The rippled graphene always emerges near the boundary of graphene. The planar graphene appears on the Cu (111) facet and the 1D and 2D rippled graphene appear on the Cu (100) and Cu (110) facets. Our measurements lead us to believe the rippled graphene is caused by the negative thermal expansion coefficient of graphene and the interaction between graphene and different Cu facets. As the sample is cooled from the annealing temperature, the graphene expands as the Cu surfaces contract. The excess graphene on Cu surfaces leads to graphene ripples. In the middle domain, the excess graphene diffuses towards planarity, while near the boundaries the spatial constraints cause rippled graphene to form. Since graphene has a stronger interaction with Cu (111) facet, graphene preferentially forms a moiré pattern on Cu (111) instead of a rippled pattern.

We deposited C_{60} molecules on both rippled and planar graphene with a low coverage, typically less than 10%. On planar graphene, C_{60} molecules self-assemble to an hcp arrangement (Fig. 2e) similar to previous studies [12,16,29]. Fig. 2f is the zoomed image of the area marked in Fig. 2e showing a moiré pattern. This moiré pattern originates from the moiré pattern of graphene and Cu (111) surface as shown in Fig. 1i. For C_{60} on rippled graphene, the C_{60} self-assembly is more complicated than that on the planar case. C_{60} molecules form a quasi-hcp structure as shown in Fig. 2a–c at various scales. The quasi-hcp structure formed on rippled graphene has a different angle from that formed on the planar area. For example, the angle shown in Fig. 2c is 54.1° instead of 60.0° shown in Fig. 2f. The angle difference between C_{60} on rippled graphene and planar graphene is due to the geometric curvature of the rippled graphene. When compared to C_{60} adsorbed on planar graphene, the hcp structure on rippled graphene is distorted by the curvature of the surface. The difference is also reflected in the corresponding Fast Fourier Transform (FFT) images (the insets in Fig. 2c and e).

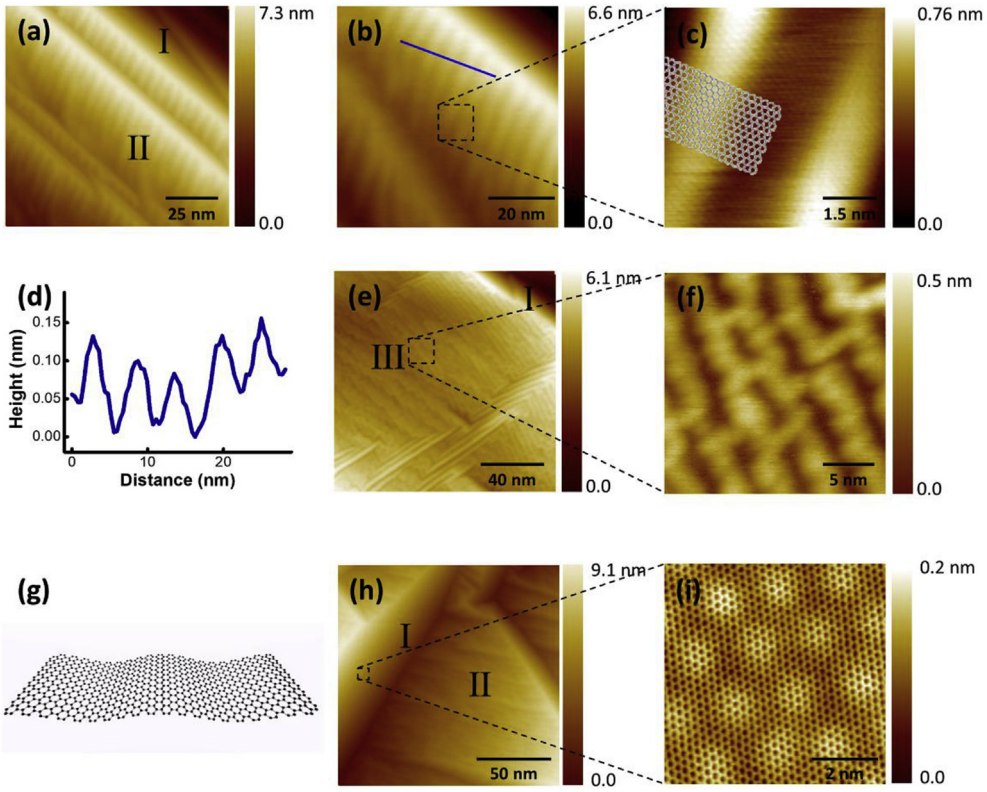

Fig. 1. (Color online) STM topographical images of planar graphene (labeled as I), 1D-rippled graphene (II) and 2D-rippled graphene (III) on Cu. (a) Large area STM image of planar graphene (I) and 1D-rippled graphene (II) showing the linear periodic modulation and the spatial modulation frequencies ($V_s = -2.340$ V, I = 0.110 nA). (b) High-resolution STM image of 1-D rippled graphene ($V_s = -0.340$ V, I = 1.900 nA). (c) STM image of the 1-D rippled graphene, observed from the square region marked in (b), the schematic model on top of the atomic image shows the ripples along zigzag direction ($V_s = -0.280$ V, I = 1.900 nA). (d) Line profile perpendicular to the 1D-rippled graphene (marked as a blue line in (b)) showing the periodic modulation. (e) STM image of graphene on two different Cu facets, planar graphene (I) and 2D-rippled graphene (III) ($V_s = -2.74$ V, I = 0.045 nA). (f) High-resolution STM image of 2D-rippled graphene, observed from the dashed square region marked in (e) ($V_s = -2.600$ V, I = 0.068 nA). (g) A schematic model shows 1D-rippled graphene sheet. (h) Large area STM image of planar graphene (I) and 1D-rippled graphene (II) ($V_s = -1.850$ V, I = 0.340 nA). (i) Atomic STM image showing the moiré pattern of planar graphene, observed from the dashed squared region marked in (h) ($V_s = -1.850$ V, I = 0.450 nA).

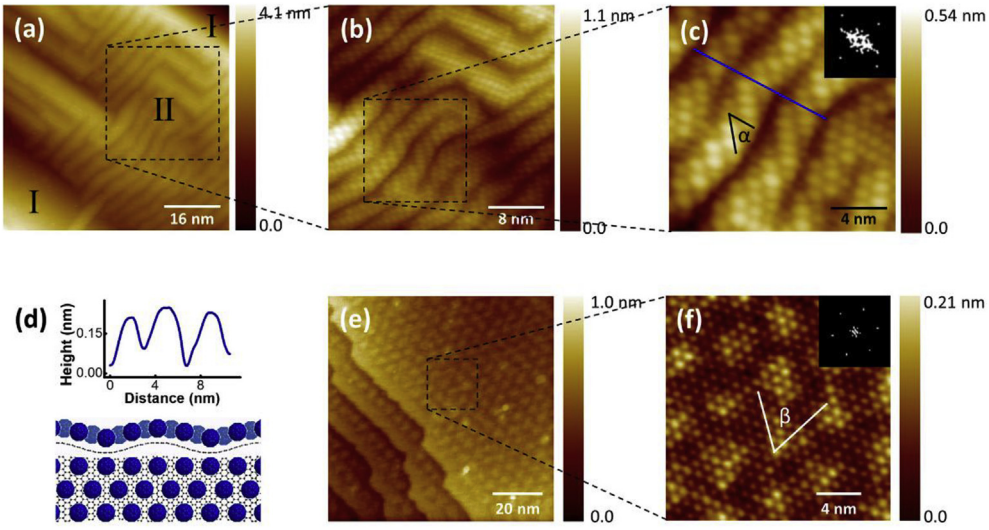

Fig. 2. (Color online) STM images of C_{60} on 1D-rippled graphene (II) and on planar graphene (I). (a) Large area STM topographic image of the C_{60} on 1D-rippled graphene showing well-defined linear periodic modulated ripple ($V_s = -2.00$ V, I = 0.060 nA). (b) Zoomed-in STM image (measured from the dashed square of (a)) of C_{60} on a long periodic graphene ripple ($V_s = -2.60$ V, I = 0.050 nA). (c) High-resolution image (measured from the dashed square region of (b)) C_{60} on 1D-rippled graphene, shows a lattice angle α of 54.1° with a quasi-hcp pattern ($V_s = -2.60$ V, I = 0.040 nA). Inset, the corresponding FFT image of (c). (d) A line profile along the perpendicular direction of the 1D-rippled graphene marked with the blue line in (c) (top), side view and top view showing the quasi-hcp C_{60} on 1D-rippled graphene (bottom). (e) Large area STM image of the C_{60} on planar graphene with a well-defined moiré pattern on facet I ($V_s = -2.65$ V, I = 0.046 nA). (f) High-resolution STM image of C_{60} on planar graphene (measured from the square region of (e)), showing a lattice angle β of 60.0° and a moiré pattern on facet I ($V_s = -2.65$ V, I = 0.046 nA). Inset, the corresponding FFT image of (f).

The difference between the C_{60} structure formed on planar graphene and rippled graphene is primarily due to the differences of van der Waals forces for peaks and valleys. Based on our DFT calculations, C_{60} will initially deposit in the valleys of rippled graphene. As additional C_{60} is deposited covering the peaks, the quasi-hcp structure is formed. DFT calculations identify the binding energy of a C_{60}-graphene valley site to be 0.34 eV more than the binding energy of a C_{60}-graphene peak site. The high-resolution STM image suggests that adsorbed C_{60} is not continuously deposited in the valleys of the 1D-rippled graphene. The C_{60} molecules are not fully revealed in the STM images because the STM tip is not sharp enough to measure into the narrow valley regions.

In order to better understand the interactions between adsorbed molecules and rippled graphene, we investigated PTCDA on 1D-rippled and planar graphene substrates. Similar to C_{60} on graphene, the coverage of PTCDA on rippled and planar areas is low, typically less than 8%. The most common arrangement for PTCDA molecules on planar graphene is a herringbone structure (Fig. 3c and d). The high resolution STM image (Fig. 3d) reveals a herringbone arrangement with $a_1 = 1.3$ nm, $a_2 = 1.96$ nm, and $\gamma = 90°$, consistent with previous reports [13,17,18,28]. The inset in Fig. 3c is the FFT image of the herringbone structure obtained from an ordered area shown as the right part of Fig. S2c. On 1D-rippled graphene, the herringbone structure of the adsorbed PTCDA molecules is influenced by the graphene curvature. In Fig. 3b, we see there are a few PTCDA herringbone structures at the top right corner, while other regions show PTCDA molecules forming a distorted herringbone pattern. The FFT images of PTCDA on rippled and planar graphene (the insets in Fig. 3b and c) also show the difference.

Our results (Fig. 3e and f and Fig. S2) further show that PTCDA sub monolayer is very easy to disassemble, due to the weak interaction between PTCDA molecule and graphene on copper substrate. During disassembly, we found a very interesting substable PTCDA structure (purple curved region shown in Fig. 3e and Fig. S2) with a rectangular lattice. This substable structure is formed by the interaction between PTCDA molecules and STM tip. After growing to a critical size, the substable PTCDA would be moved away by the tip (Figs. S2g and S2h).

When compared to planar graphene, molecules adsorbed onto 1D-rippled graphene show different patterns. To obtain further understanding of the formation mechanism we have calculated the magnitude of the adsorbed molecule/curved graphene interaction. We employed computational approaches based on DFT with van der Waals dispersion corrections to explore the interactions between C_{60} molecules and the curved graphene surface. As previously noted [46], the potential energy of C_{60}-graphene complex is sensitive to C_{60} molecular orientation on the graphene surface. Previous work established that the energy minima of different C_{60} orientations are similar and are in the range of rotation energy barriers [43]. Inspired by previous studies, we inspect typical orientations (described in the Supporting Information). A detailed examination of typical C_{60} orientations is employed to investigate the effects of orientations and to find the most stable configuration. It has been confirmed that the offset face-to-face alignment (Supporting Information Fig. S2 b) is energetically favored and shows an ~1 kcal/mol lower energy than other orientations [47,48]. As shown in Fig. 4 (a,b), there are two archetype locations on curved graphene surface for arranging C_{60} molecules, the peak and the valley. C_{60} molecules located on the peak area may be modeled with a C_{60} on a convex aromatic surface and C_{60} molecules located in the valley area may be modeled with a C_{60} on a concave aromatic surface. A previous computational study revealed that C_{60} molecules on a concave aromatic surface have larger intermolecular interactions which provide greater stability [43]. As illustrated in Fig. 4d, a C_{60} molecule located on a graphene peak has a relative interaction energy of −0.92 eV while the interaction energy for C_{60} in a graphene valley is −1.26 eV. The relative interaction energy for C_{60} and planar graphene falls in between with a value of −1.07 eV. Calculations reveal an optimized C_{60} molecule − curved graphene distance of 3.1 Å. The energy curves shown in Fig. 4.d show a significant energy difference between C_{60} molecules located on a peak and those located in a valley. Fig. 5 shows results of DFT calculations for adsorbed molecule-graphene interactions. The curved graphene structure increases the stability for C_{60} molecules in valley regions. The additional stability leads to the self-assembled

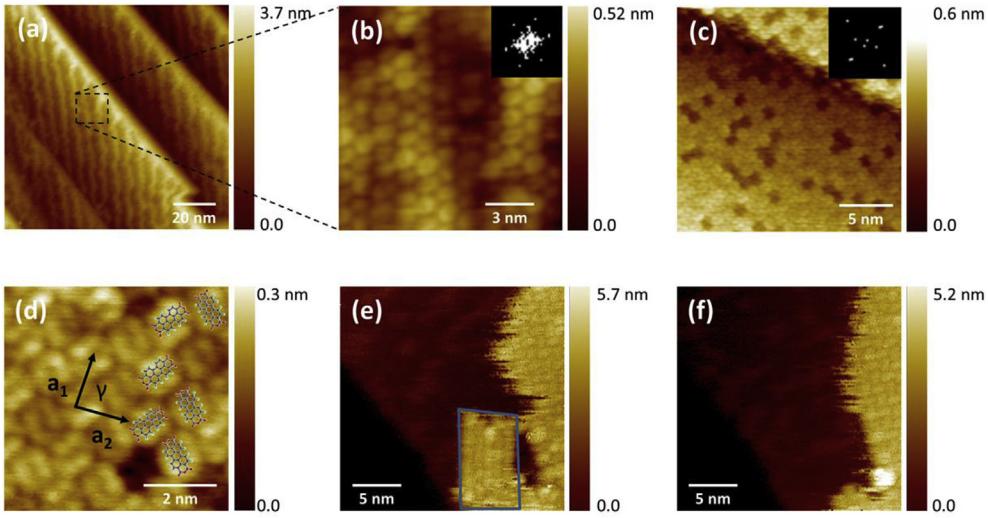

Fig. 3. (Color online) STM images of PTCDA on 1D-rippled graphene and on planar graphene. (a) Large area STM image of PTCDA on 1D-rippled graphene ($V_s = -2.51$ V, $I = 0.042$ nA). (b) STM image of PTCDA on 1D-rippled graphene showing a distorted herringbone pattern ($V_s = -2.510$ V, $I = 0.042$ nA). Inset, the corresponding FFT image of (b). (c) Large area STM image of PTCDA on planar graphene ($V_s = 1.800$ V, $I = 0.030$ nA). Inset, the FFT image of the PTCDA herringbone structure on planar graphene. (d) Zoomed-in STM image of PTCDA on planar graphene; a_1 and a_2 indicate the short and long lattice vectors of a unit cell of the PTCDA herringbone pattern ($V_s = 1.800$ V, $I = 0.030$ nA). (e) STM images of coexistence of substable PTCDA structure (purple curved region) and normal PTCDA herringbone structure ($V_s = -2.500$ V, $I = 0.030$ nA). (f) STM image of remaining normal PTCDA structure after the substable PTCDA removed by STM tip ($V_s = -2.500$ V, $I = 0.030$ nA).

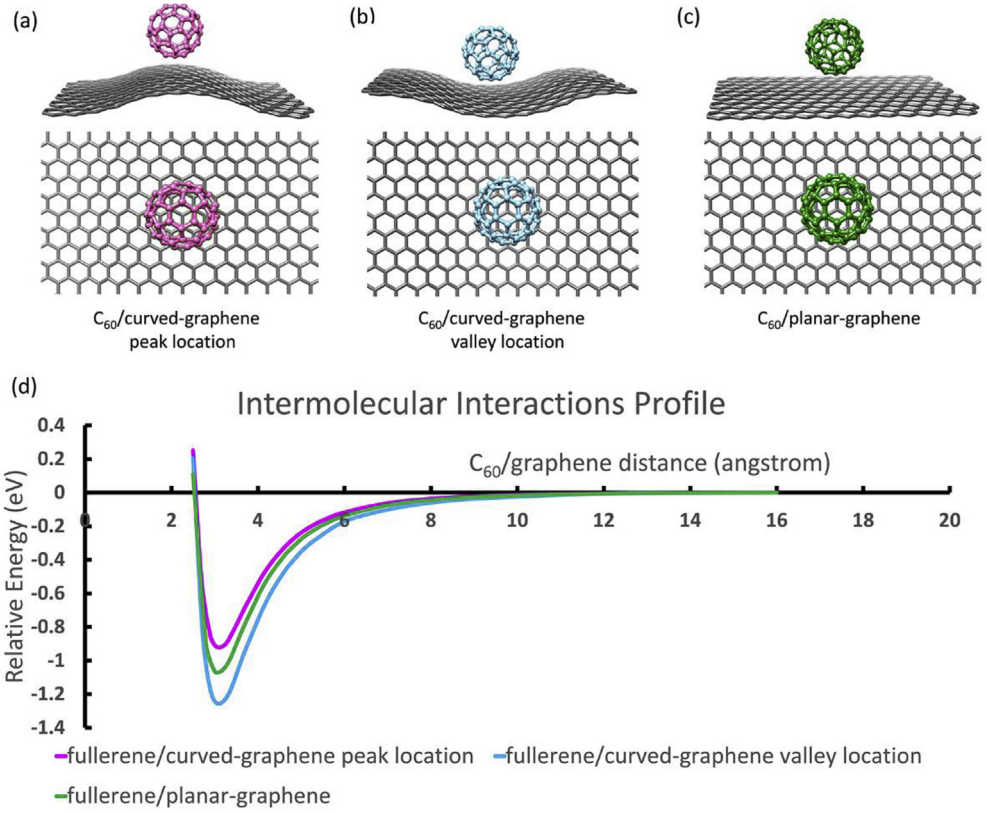

Fig. 4. (Color online) Computational results for C_{60} on 1D-rippled graphene and planar graphene showing energetically favored orientations. (a) C_{60} molecule on a peak site on curved-graphene, (b) C_{60} molecule with a valley site on curved-graphene and (c) C_{60} on planar-graphene. (d) Plot of C_{60}-graphene distance versus relative energy for C_{60} on a graphene peak (pink), C_{60} in a graphene valley (blue) and C_{60} on planar graphene (green).

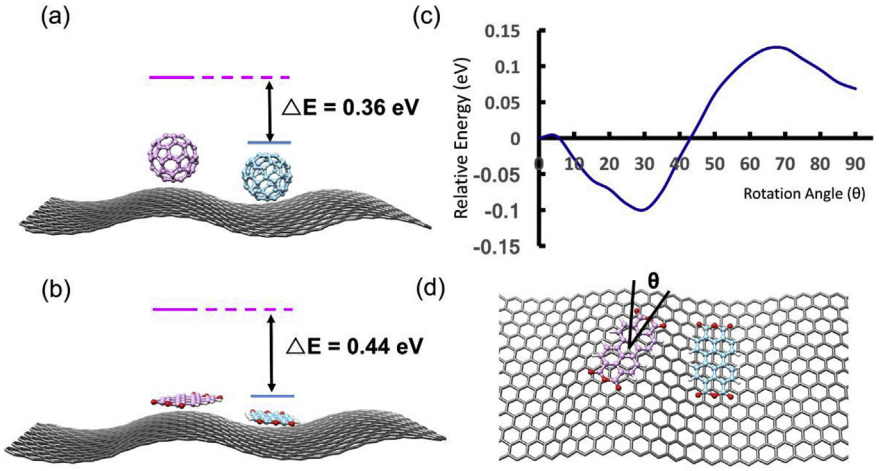

Fig. 5. (Color online) DFT results for adsorbed molecule/graphene interactions. (a) Energy difference of a C_{60} molecule on a 1D-rippled graphene surface (b) Energy difference of a PTCDA molecule on a 1D-rippled graphene. (c) Energy curve for a PTCDA molecule rotation on 1D-rippled graphene on a peak location (top); favored PTCDA orientations (bottom). (d) Favored PTCDA orientations at the peak site (left) and at the valley site (right).

quasi-hcp configurations of C_{60} molecules on the 1D-rippled graphene surface.

In contrast to the hcp pattern for C_{60} molecules on a planar graphene surface, it has been shown that PTCDA molecules form herringbone structure on a planar graphene surface. However, on a 1D-rippled graphene surface, we observed disordered herringbone pattern for the PTCDA molecules. The disordered structure implies that the curved graphene surface has a significant effect on the self-assembly of the PTCDA molecules. We utilized DFT-based calculations to obtain further understanding on the structures of a PTCDA molecule on a 1D-curved graphene surface. Our calculations show the relative energies between PTCDA and curved graphene on a peak and in a valley are −2.17 eV and −2.61 eV, respectively. This may be compared to a relative energy of −2.40 eV for PTCDA on planar graphene. Calculations reveal that PTCDA molecules prefer different orientations on a graphene peak and in a graphene valley

as shown in Fig. 5a and b. A PTCDA molecule in a valley aligns symmetrically while the lowest relative energy for a molecule on a graphene peak makes a 30° angle with the ridge (Fig. 5c). A possible explanation for the angle is the electronegative oxygens minimizing contact with the graphene while maximizing π-π stacking interactions. The difference in preferred orientations for PTCDA molecules on peaks and in valleys show that curved graphene may be used to help to regulate the orientation of molecules. Compared to the C_{60}/curved graphene interaction, the PTCDA/curved graphene interactions are slightly stronger due to larger contact area between PTCDA molecules and the curved graphene. In both cases, adsorbed molecules in valley sites show a stronger interaction than the same molecule adsorbed on planar graphene.

4. Conclusions

In this paper we have demonstrated the self-assembly of C_{60} and PTCDA molecules on rippled graphene with characterization using both experimental STM and DFT calculations. The adsorbed molecules on 1D-rippled graphene systems reveal distortions when compared with analogous planar graphene system. Specifically, the nearly spherical I_h-symmetrical C_{60} molecules form a quasi-hexagonal close packed structure, while the planar PTCDA molecules form a disordered herringbone structure on the rippled graphene surface. The change in the monolayer packing pattern of C_{60} and PTCDA molecules on a curved graphene surface is due to competition between the adsorbate-graphene interaction and the intermolecular adsorbate interactions. Because of the nearly spherical C_{60} molecules, the rippled graphene surface exhibits only diminished effects on the π-π intermolecular interactions. In contrast, the planar PTCDA molecules have different sides for intermolecular interactions, namely, sp^2 hybridized on opposite two sides and significantly more electronegative oxygen anhydride moieties on the other two sides. This leads to the well characterized herringbone structure that is assembled mainly based on the relative weak PTCDA hydrogen bonds, C-H•••O, with a strength estimated as 0.1 eV. In this case, the PTCDA-graphene interaction, which have energies at the peak and valley sites of 2.17 and 2.61 eV, respectively, are far more important than the PTCDA intermolecular interaction. These results are also consistent with the tendency for dissembling the PTCDA submonolayer *vide supra*. Furthermore, the DFT computational results demonstrate significant increases in π-π interactions for both the adsorbed PTCDA and C_{60}/rippled graphene complexes located in the 2D graphene valley sites in comparison with adsorbed more idealized molecule/planar graphene 2D complexes. In addition, we find that the adsorbed planar PTCDA molecules prefer different orientations when the rippled graphene peak regions are compared to the valley regions. These fundamental experimental and computational results are important for understanding any potential application of structurally diverse molecules adsorbed on graphene and/or rippled graphene surfaces.

Acknowledgements

Y.L., C.C. and C.T. acknowledge the financial support provided for this work by the U.S. Army Research Office under the grant W911NF-15-1-0414. T.F.C. and Y.P.C. acknowledge partial support by NSF CMMI (grant 1538360) and EFMA (grant 1641101) on graphene synthesis at Purdue University.

Appendix A. Supplementary data

Supplementary data to this article can be found online at https://doi.org/10.1016/j.carbon.2019.01.070.

References

[1] K.S. Novoselov, A.K. Geim, S.V. Morozov, D. Jiang, M.I. Katsnelson, I.V. Grigorieva, S.V. Dubonos, A.A. Firsov, Two-dimensional gas of massless Dirac fermions in graphene, Nature 438 (7065) (2005) 197–200.
[2] Y.B. Zhang, Y.W. Tan, H.L. Stormer, P. Kim, Experimental observation of the quantum Hall effect and Berry's phase in graphene, Nature 438 (7065) (2005) 201–204.
[3] A.H. Castro Neto, F. Guinea, N.M.R. Peres, K.S. Novoselov, A.K. Geim, The electronic properties of graphene, Rev. Mod. Phys. 81 (1) (2009) 109–162.
[4] T. Georgiou, R. Jalil, B.D. Belle, L. Britnell, R.V. Gorbachev, S.V. Morozov, Y.J. Kim, A. Gholinia, S.J. Haigh, O. Makarovsky, L. Eaves, L.A. Ponomarenko, A.K. Geim, K.S. Novoselov, A. Mishchenko, Vertical field-effect transistor based on graphene-WS_2 heterostructures for flexible and transparent electronics, Nat. Nanotechnol. 8 (2) (2013) 100–103.
[5] Y.H. Kim, S.J. Kim, Y.J. Kim, Y.S. Shim, S.Y. Kim, B.H. Hong, H.W. Jang, Self-activated transparent all-graphene gas sensor with endurance to humidity and mechanical bending, ACS Nano 9 (10) (2015) 10453–10460.
[6] M.A. Sentef, M. Claassen, A.F. Kemper, B. Moritz, T. Oka, J.K. Freericks, T.P. Devereaux, Theory of Floquet band formation and local pseudospin textures in pump-probe photoemission of graphene, Nat. Commun. 6 (2015), 7047(1-8).
[7] A.K. Geim, Graphene: status and prospects, Science 324 (5934) (2009) 1530–1534.
[8] A. Zurutuza, C. Marinelli, Challenges and opportunities in graphene commercialization, Nat. Nanotechnol. 9 (10) (2014) 730–734.
[9] P. Avouris, F.N. Xia, Graphene applications in electronics and photonics, MRS Bull. 37 (12) (2012) 1225–1234.
[10] W.Z. Bao, F. Miao, Z. Chen, H. Zhang, W.Y. Jang, C. Dames, C.N. Lau, Controlled ripple texturing of suspended graphene and ultrathin graphite membranes, Nat. Nanotechnol. 4 (9) (2009) 562–566.
[11] M. Ishigami, J.H. Chen, W.G. Cullen, M.S. Fuhrer, E.D. Williams, Atomic structure of graphene on SiO_2, Nano Lett. 7 (6) (2007) 1643–1648.
[12] G. Li, H.T. Zhou, L.D. Pan, Y. Zhang, J.H. Mao, Q. Zou, H.M. Guo, Y.L. Wang, S.X. Du, H.J. Gao, Self-assembly of C_{60} monolayer on epitaxially grown, nanostructured graphene on Ru(0001) surface, Appl. Phys. Lett. 100 (1) (2012), 013304(1-4).
[13] Q.H. Wang, M.C. Hersam, Room-temperature molecular-resolution characterization of self-assembled organic monolayers on epitaxial graphene, Nat. Chem. 1 (3) (2009) 206–211.
[14] J.M. MacLeod, F. Rosei, Molecular self-assembly on graphene, Small 10 (6) (2014) 1038–1049.
[15] P. Jarvinen, S.K. Hamalainen, M. Ijas, A. Harju, P. Liljeroth, Self-assembly and orbital imaging of metal phthalocyanines on a graphene model surface, J. Phys. Chem. C 118 (24) (2014) 13320–13325.
[16] C.H. Chen, H.S. Zheng, A. Mills, J.R. Heflin, C.G. Tao, Temperature evolution of quasi-one-dimensional C_{60} nanostructures on rippled graphene, Sci. Rep. 5 (2015), 14336(1-7).
[17] A.J. Martinez-Galera, N. Nicoara, J.I. Martinez, Y.J. Dappe, J. Ortega, J.M. Gomez-Rodriguez, Imaging molecular orbitals of PTCDA on graphene on Pt(111): electronic structure by STM and first-principles calculations, J. Phys. Chem. C 118 (24) (2014) 12782–12788.
[18] J.D. Emery, Q.H. Wang, M. Zarrouati, P. Fenter, M.C. Hersam, M.J. Bedzyk, Structural analysis of PTCDA monolayers on epitaxial graphene with ultra-high vacuum scanning tunneling microscopy and high-resolution X-ray reflectivity, Surf. Sci. 605 (17–18) (2011) 1685–1693.
[19] J. Lu, P.S.E. Yeo, Y. Zheng, Z.Y. Yang, Q.L. Bao, C.K. Gan, K.P. Loh, Using the graphene moire pattern for the trapping of C_{60} and homoepitaxy of graphene, ACS Nano 6 (1) (2012) 944–950.
[20] N.S. Sariciftci, L. Smilowitz, A.J. Heeger, F. Wudl, Photoinduced electron-transfer from a conducting polymer to buckminsterfullerene, Science 258 (5087) (1992) 1474–1476.
[21] S. Morita, A.A. Zakhidov, K. Yoshino, Doping effect of buckminsterfullerene in conducting polymer - change of absorption-spectrum and quenching of luminescence, Solid State Commun. 82 (4) (1992) 249–252.
[22] L. Smilowitz, N.S. Sariciftci, R. Wu, C. Gettinger, A.J. Heeger, F. Wudl, Photoexcitation spectroscopy of conducting-polymer-C_{60} composites - photoinduced electron-transfer, Phys. Rev. B 47 (20) (1993) 13835–13842.
[23] P. Peumans, A. Yakimov, S.R. Forrest, Small molecular weight organic thin-film photodetectors and solar cells, J. Appl. Phys. 93 (7) (2003) 3693–3723.
[24] B.P. Rand, D.P. Burk, S.R. Forrest, Offset energies at organic semiconductor heterojunctions and their influence on the open-circuit voltage of thin-film solar cells, Phys. Rev. B 75 (11) (2007), 115327(1-11).
[25] L. Meng, Y. Zhang, X. Wan, C. Li, X. Zhang, Y. Wang, X. Ke, Z. Xiao, L. Ding, R. Xia, H.-L. Yip, Y. Cao, Y. Chen, Organic and solution-processed tandem solar cells with 17.3% efficiency, Science 361 (6407) (2018) 1094–1098.
[26] X. Wang, L.J. Zhi, K. Mullen, Transparent, conductive graphene electrodes for dye-sensitized solar cells, Nano Lett. 8 (1) (2008) 323–327.
[27] J.B. Wu, H.A. Becerril, Z.N. Bao, Z.F. Liu, Y.S. Chen, P. Peumans, Organic solar cells with solution-processed graphene transparent electrodes, Appl. Phys. Lett. 92 (26) (2008), 263302(1-3).
[28] H. Huang, S. Chen, X.Y. Gao, W. Chen, A.T.S. Wee, Structural and electronic properties of PTCDA thin films on epitaxial graphene, ACS Nano 3 (11) (2009) 3431–3436.

[29] J. Cho, J. Smerdon, L. Gao, O. Suzer, J.R. Guest, N.P. Guisinger, Structural and electronic decoupling of C_{60} from epitaxial graphene on SiC, Nano Lett. 12 (6) (2012) 3018–3024.
[30] J.U. Reveles, N.N. Karle, T. Baruah, R.R. Zope, Electronic and structural properties of C_{60} and $Sc3N@C_{80}$ supported on graphene nanoflakes, J. Phys. Chem. C 120 (45) (2016) 26083–26092.
[31] B.K. Mishra, J.S. Arey, N. Sathyamurthy, Stacking and spreading interaction in N-heteroaromatic systems, J. Phys. Chem. 114 (36) (2010) 9606–9616.
[32] B.W. Gung, F. Wekesa, C.L. Barnes, Stacking interactions between nitrogen-containing six-membered heterocyclic aromatic rings and substituted benzene: studies in solution and in the solid state, J. Org. Chem. 73 (5) (2008) 1803–1808.
[33] L. Tapaszto, T. Dumitrica, S.J. Kim, P. Nemes-Incze, C. Hwang, L.P. Biro, Breakdown of continuum mechanics for nanometre-wavelength rippling of graphene, Nat. Phys. 8 (10) (2012) 739–742.
[34] J.F. Tian, H.L. Cao, W. Wu, Q.K. Yu, N.P. Guisinger, Y.P. Chen, Graphene induced surface reconstruction of Cu, Nano Lett. 12 (8) (2012) 3893–3899.
[35] K.K. Bai, Y. Zhou, H. Zheng, L. Meng, H.L. Peng, Z.F. Liu, J.C. Nie, L. He, Creating one-dimensional nanoscale periodic ripples in a continuous mosaic graphene monolayer, Phys. Rev. Lett. 113 (8) (2014), 086102(5).
[36] S.K. Deng, V. Berry, Wrinkled, rippled and crumpled graphene: an overview of formation mechanism, electronic properties, and applications, Mater. Today 19 (4) (2016) 197–212.
[37] Q.K. Yu, L.A. Jauregui, W. Wu, R. Colby, J.F. Tian, Z.H. Su, H.L. Cao, Z.H. Liu, D. Pandey, D.G. Wei, T.F. Chung, P. Peng, N.P. Guisinger, E.A. Stach, J.M. Bao, S.S. Pei, Y.P. Chen, Control and characterization of individual grains and grain boundaries in graphene grown by chemical vapour deposition, Nat. Mater. 10 (6) (2011) 443–449.
[38] H. Kruse, S. Grimme, A geometrical correction for the inter- and intra-molecular basis set superposition error in Hartree-Fock and density functional theory calculations for large systems, J. Chem. Phys. 136 (15) (2012), 154101(16).
[39] A. Schafer, H. Horn, R. Ahlrichs, Fully optimized contracted Gaussian-basis sets for atoms Li to Kr, J. Chem. Phys. 97 (4) (1992) 2571–2577.
[40] A. Schafer, C. Huber, R. Ahlrichs, Fully optimized contracted Gaussian-basis sets of triple zeta valence quality for atoms Li to Kr, J. Chem. Phys. 100 (8) (1994) 5829–5835.
[41] S. Grimme, Semiempirical GGA-type density functional constructed with a long-range dispersion correction, J. Comput. Chem. 27 (15) (2006) 1787–1799.
[42] S. Grimme, S. Ehrlich, L. Goerigk, Effect of the damping function in dispersion corrected density functional theory, J. Comput. Chem. 32 (7) (2011) 1456–1465.
[43] E.M. Cabaleiro-Lago, J. Rodriguez-Otero, J.A. Carrazana-Garcia, A theoretical study of complexes between fullerenes and concave receptors with interest in photovoltaics, Phys. Chem. Chem. Phys. 19 (39) (2017) 26787–26798.
[44] I. Gonzalez-Veloso, J. Rodriguez-Otero, E.M. Cabaleiro-Lago, Carbon-nanorings ([10]CPP and [6]CPPA) as fullerene (C_{60} and C_{70}) receptors: a comprehensive dispersion-corrected DFT study, Phys. Chem. Chem. Phys. 18 (46) (2016) 31670–31679.
[45] L. Gao, J.R. Guest, N.P. Guisinger, Epitaxial graphene on Cu(111), Nano Lett. 10 (9) (2010) 3512–3516.
[46] C. Ojeda-Aristizabal, E.J.G. Santos, S. Onishi, A.M. Yan, H.I. Rasool, S. Kahn, Y.C. Lv, D.W. Latzke, J. Velasco, M.F. Crommie, M. Sorensen, K. Gotlieb, C.Y. Lin, K. Watanabe, T. Taniguchi, A. Lanzara, A. Zettl, Molecular arrangement and charge transfer in C_{60}/graphene heterostructures, ACS Nano 11 (5) (2017) 4686–4693.
[47] T.F. Headen, C.A. Howard, N.T. Skipper, M.A. Wilkinson, D.T. Bowron, A.K. Soper, Structure of pi-pi interactions in aromatic liquids, J. Am. Chem. Soc. 132 (16) (2010) 5735–5742.
[48] C. Feng, C.S. Lin, W. Fan, R.Q. Zhang, M.A. Van Hove, Stacking of polycyclic aromatic hydrocarbons as prototype for graphene multilayers, studied using density functional theory augmented with a dispersion term, J. Chem. Phys. 131 (19) (2009), 194702(8).